PERGAMON

International Journal of Heat and Mass Transfer 42 (1999) 3113–3129

International Journal of HEAT and MASS TRANSFER

Heat transfer to liquid drops passing through an immiscible liquid medium between tilted parallel-plate electrodes

T. Mochizuki[a,*], T. Nozaki[b], Y.H. Mori[b], N. Kaji[c]

[a]Department of Technology Education, Tokyo Gakugei University, 4-1-1 Nukuikitamachi, Koganei-shi, Tokyo 184-8501, Japan
[b]Department of Mechanical Engineering, Keio University, 3-14-1 Hiyoshi, Kouhoku-ku, Yokohama 223-8522, Japan
[c]Department of Mechanical Engineering, The Polytechnic University, 4-1-1 Hashimoto-dai, Sagamihara 229-1196, Japan

Received 12 May 1998; received in revised form 10 November 1998

Abstract

This paper describes an experimental examination of a novel scheme of enhancing heat (or mass) transfer in liquid–liquid dispersed systems: one liquid is released in the form of drops into a continuous medium of another immiscible, less electrically-conducting liquid which is confined by a pair of parallel-plate electrodes tilted from the vertical. Each drop is driven by a Coulombic force to bounce back and forth between the electrodes while falling down (or rising up) along the axis of tilt of the electrodes due to gravity, thereby following a zigzag trajectory. An increase in the strength of the electric field should enhance the instantaneous heat transfer to or from the drop, while an increase in the tilt angle of the electrodes should lengthen the drop-medium contact time. The heat transfer to single water drops passing through a silicone-oil medium between a pair of tilted parallel-plate electrodes has been studied by use of a thermochromic liquid–crystal thermometry technique.

1. Introduction

If a liquid drop released in an immiscible dielectric–liquid medium confined by a pair of parallel-plate electrodes has a net charge and is subjected to an electric field across the electrode spacing, the drop will migrate toward either one of the electrodes which is opposite in polarity to the charge on the drop, and will collide with the electrode. The collision should cause a charge exchange between the drop and the electrode. The drop thus recharged to the same polarity as the electrode will inevitably be repulsed from the electrode toward the opposite one. If the drop does not lose the charge on it during its transit of the electrode spacing, it will fall into successive bouncing motions between the electrodes. The average translational velocity of the drop in such Coulombic-force-driven bouncing motions can be significantly higher than the terminal velocity that the same drop would have in the absence of the electric field. The potential utility of the above electrohydrodynamic principle in liquid-to-liquid heat/mass transfer operations was first noted by Mori and Kaji [1]. This idea was tested in Kaji et al. [2] with single water drops rising in a denser methylphenyl silicone oil confined by a pair of vertically oriented parallel-plate electrodes. It was found that the coefficient of medium-to-drop heat transfer can be increased by a

* Corresponding author.

0017-9310/99/$ - see front matter
PII: S0017-9310(98)00381-0

Nomenclature

A	area of contact (in macroscopic sense) between drop and electrode
c_p	specific heat capacity
C_D	drag coefficient
D, D_0	diameter of electrically conducting sphere and volume-equivalent spherical diameter of drop
D_n, D_p	drop axes normal and parallel to electric field, respectively
$\boldsymbol{E}$, E_n	electric field vector and nominal field strength ($\equiv\lvert V\rvert/l$), respectively
F	temperature effectiveness for drops
$\boldsymbol{F}_D$, $\boldsymbol{F}_E$	drag force and Coulombic force working on drop, respectively
F_l	magnitude of force with which silicone oil layer intervening between drop and electrode presses the area A
$\boldsymbol{g}$	acceleration due to gravity
H, H_0	hue angle and constant term in the expression for H
l	spacing between parallel plate electrodes
Nu, Nu_c, Nu_d	Nusselt numbers defined as $\alpha D/\lambda_c$, $\alpha_c D/\lambda_c$ and $\alpha_d D/\lambda_d$, respectively
Pe	Péclét number, $\equiv Re\ Pr$
Pr	Prandtl number, $\equiv c_{pc}\rho_c\nu_c/\lambda_c$
q	heat flux at drop surface included in area A
Q	net electric charge on drop
Q_t	amount of heat conducted into drop through area A
r, g, b	normalized chromaticity coordinates
R, G, B	chromaticity coordinates
Re	Reynolds number, $\equiv\lvert\boldsymbol{v}\rvert D/\nu_c$
S	saturation value
t	time
t_0, t_1	times of inception and termination, respectively, of drop-to-electrode collision
T	temperature
T_c	undisturbed temperature in continuous phase
T_d	drop temperature determined by TLC thermometry
T_{d0}	drop temperature at $t=t_0$
T_{dm}	mixed mean temperature of drop
$\boldsymbol{v}$	instantaneous drop velocity
$\bar{v}_t$	mean translational velocity
$\bar{v}_x$	mean axial velocity of drop
V	potential difference between parallel plate electrodes
x, y	coordinates defined in Fig. 3
y_c	y-axial location of geometrical center of drop

Greek symbols

α	instantaneous heat transfer coefficient related to temperature difference given by T_c-T_{dm}
α'	instantaneous heat transfer coefficient related to temperature difference given by T_c-T_d
$\bar{\alpha}$	value of α averaged over each round trip of drop across the electrode spacing
δ	thickness of silicone oil layer intervening between drop and electrode
δ_c	value of δ critical for dielectric breakdown of silicone oil layer
δ_e	thickness of electrode plate
Δt	time increment used in numerically integrating Eq. (A5)
Δy	interval of nodal-points used in integrating Eq. (A5)
ε	electrical permittivity
θ	tilt angle of electrodes from vertical
λ	thermal conductivity
Λ_x	axial distance traveled by a drop during its one round trip across the electrode spacing
ν	kinematic viscosity
ρ	mass density

σ	interfacial tension
τ	period of one round trip of drop across electrode spacing
χ	electrical resistivity
Subscripts	
b	brass (material of electrodes)
c	continuous phase (silicone oil)

few times as the result of the Coulombic-force-driven bouncing motions. Later the heat transfer to a train of drops exhibiting such bouncing motions was examined by Mochizuki et al. [3].

The bouncing motions generally tend to decrease the axial velocity (i.e., the rise or fall velocity) of drops only slightly. If we wish to substantially reduce the axial velocity (the axial component of translational velocity) of individual drops in a liquid–liquid contactor, without reducing the magnitude of their translational velocity, and hence shorten the axial length of the contactor required to achieve a high level of dispersed-phase-side temperature effectiveness or mass transfer efficiency, the most promising solution may be to tilt the contactor together with the electrodes inside it from the vertical, thereby reducing the axial component of the gravity. The idea of tilting the parallel-plate electrodes goes back to Kaji and Mori [4], who attempted to elongate the residence time, in an electrostatic drier, of solid particles to be dried while bouncing back and forth between the electrodes through a gaseous medium. The application of this idea to liquid–liquid dispersed systems is the topic of our studies, including the present one, in this series. Prior to the present study, we have investigated liquid-drop motions in another liquid in a space which may simulate a 'module' of a tilted spray-column-type contactor (e.g. direct-contact heat exchanger or extractor) equipped with multiple electrodes set parallel to the contactor axis. First, we observed the bouncing motions of single water drops in a medium of a dimethyl silicone oil confined by a pair of tilted parallel-plate electrodes, and showed that these motions are predictable to a reasonable accuracy by using a simple mechanistic model [5]. Successively we examined the mutual interactions of drops periodically released from nozzles into an electrode spacing to evaluate the minimum of initial drop intervals beyond which neighboring drops may collide and coalesce into larger drops and thereby hinder the stable operation of the contactor [6,7]. The results of these drop-motion studies were then utilized to simulate the performance, as heat exchangers, of multi-electrode contactors [8]. This simulation study was quite tentative in nature, because the medium-to-drop heat transfer was approximated, with no direct verification of its validity, by use of existing empirical correlations for the quasi-steady heat transfer to isolated solid spheres.

This paper describes our first attempt to experimentally investigate the heat transfer to individual drops. The attempt has been accomplished by applying a liquid–crystal thermometry technique [9] to measuring instantaneous temperature of each drop bouncing between tilted parallel-plate electrodes. Also presented in the paper is a simple analytic model of the heat transfer. Some predictions of heat-transfer characteristics based on the model are compared with relevant experimental results.

2. Experiments

2.1. Experimental apparatus and its operation

The experiments were so planned as to enable evaluation of quasi-steady coefficient of heat transfer to single drops passing through a test section, which was a liquid-filled rectangular space confined by a pair of tilted parallel-plate electrodes. During its passing through the test section, each drop follows a zigzag trajectory, periodically moving back and forth across the spacing between the electrodes in the presence of an electric field exceeding some critical strength. The temperature in the liquid medium in the test section is uniform and constant because of its sufficiently large heat capacity and a sufficiently long interval of drops passing through the test section. Thus, the medium-to-drop heat-transfer coefficient can be determined by only knowing the temperature history of each drop during its passage of the test section. However, the necessity for successive measurement of the instantaneous temperature of a drop moving zigzag at a high speed poses a technical difficulty.

In the present experiments, we intended to overcome the above difficulty by suspending microcapsules of thermochromic liquid crystal (TLC) in a drop-forming liquid, water, and by video-recording the color images of each drop under an invariable optical condition. This attempt was essentially dependent on a recent development of quantitative TLC thermometry for drop-temperature measurements described in Nozaki et al. [9]. Except for the optical setup for acquiring and

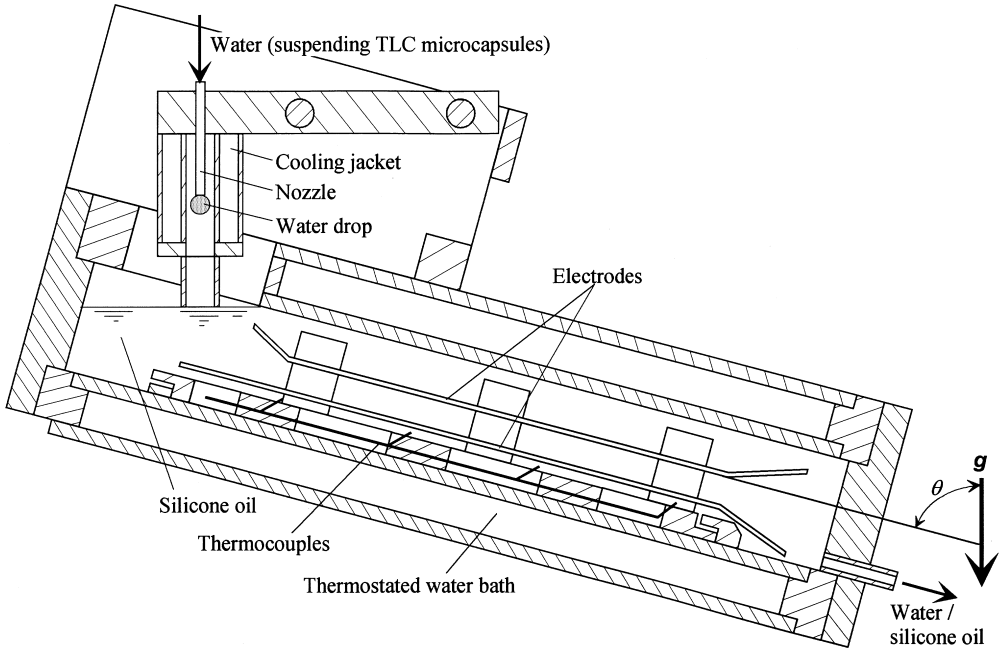

Fig. 1. Structure of test column.

processing drop images, the experimental apparatus used in the present experiments was almost the same as the one described in Ref. [5]. Some details of the major portion of the apparatus used this time are given below.

Fig. 1 schematically illustrates the test column which is a rectangular column holding a pair of parallel-plate electrodes. It was sheathed in a water jacket through which temperature-controlled water was circulated. Unlike the test column used in the previous drop-motion studies [5–7], the one used this time was fabricated of black-colored PMMA [poly(-methyl methacrylate)] plates except for its front wall which was a colorless, transparent PMMA plate. The water jacket enclosing the test column was made of colorless, transparent PMMA plates. Each electrode was a brass plate, 70-mm wide and 2-mm thick. The length of the parallel section of the paired electrodes was 360 mm. The spacing between the electrodes over the parallel section, l, was fixed at either 25 or 40 mm. The electrodes were completely immersed in a dimethyl silicone oil [KF96(10cst) fluid prepared by Shin-etsu Chemical Co., Tokyo] which almost filled the column. It should be noted that before setting in the column, the electrodes were baked once in an electric furnace, after being wetted with the same silicone oil as the one to be poured in the column. This treatment of the electrodes made their surfaces hydrophobic enough to prevent drops of water, suspending TLC microcapsules, from sticking to the electrodes. The electrode at a lower position was always grounded, while a positive potential, V, was applied to the opposite electrode from a Spellman 30PN30 high-voltage direct-current power supply. Four thermocouples were axially aligned behind the grounded electrode to monitor the temperature of the silicone oil.

A nozzle assembly for releasing drops of water suspending TLC microcapsules into the silicone oil medium was inserted into the test column through an opening at the upper end of the column. The nozzle itself was a stainless-steel tube having a tip cut at right angles to its axis. The tube size was 6 mm OD and 5 mm ID or 0.41 mm OD and 0.20 mm ID, depending on the desired size of drops to be released from the nozzle. The nozzle was sheathed concentrically with a cooling jacket, through which circulated the water having flowed out of the jacket enclosing the reservoir of the drop-forming liquid, i.e., water suspending TLC microcapsules, as explained later. The nozzle was oriented vertically, irrespective of how the test column was tilted, and, unlike the one used in the previous studies, it was held above the free surface of the silicone oil in the column such that drops were formed in the air and dripped into the silicone oil. This nozzle arrangement enabled the release of drops of constant size irrespective of θ, the angle of tilt of the column from vertical, while minimizing the indefinite tempera-

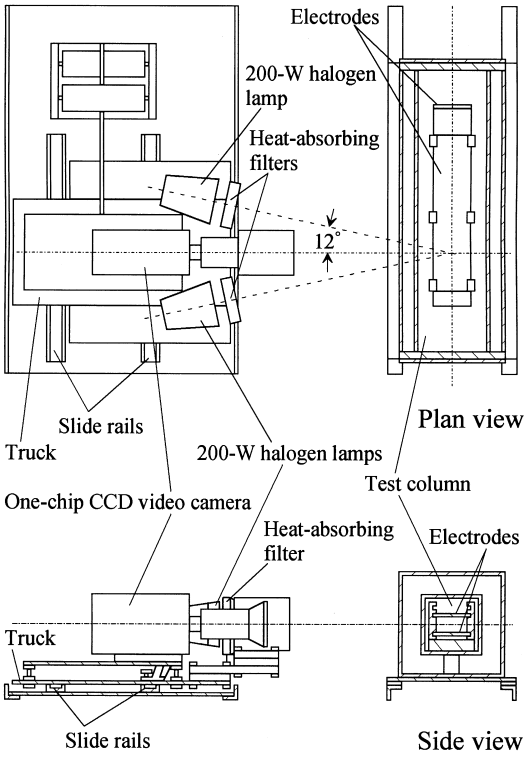

Fig. 2. Arrangement of test column and video-camera assembly.

ture change of each drop before its detachment from the nozzle.

The drop-forming liquid was prepared and stored in a PMMA-made cylindrical reservoir, in which distilled water and TLC microcapsules (KWWN-4555 prepared by Japan Capsular Products Inc., Tokyo) added at 0.5 wt% to the water were continuously agitated with the aid of a stirrer. The TLC microcapsules were ~15 μm in diameter, each encapsulating a chiral nematic liquid crystal with an ureaformaldehyde resin film. The temperature in the reservoir was controlled by circulating water through the jacket enclosing the reservoir. The TLC suspension in the reservoir was supplied to the nozzle by a tubing roller pump.

Special attention was paid in the arrangement of the test column and the video-camera assembly such as to produce drop images competent for a quantitative image analysis. The test column was mounted on a highly rigid, missile-launcher-shaped steel platform whose angle of slope could be adjusted as desired. A one-chip CCD video camera and two 200-W halogen lamps (3200 K color temperature) with heat-absorbing filters were mounted together, as illustrated in Fig. 2,

Table 1
Operational range of experiments

D_0 [mm]	l [mm]	θ [deg]	E_n [MV m^{-1}]
5.5	25	0–73	0.15–0.30
5.5	40	45	0.16–0.30
3.7	25	45	0.16–0.38

on a truck movable on a pair of parallel rails which were fixed onto another platform, the same size and geometry as the one supporting the test column. The two platforms were set parallel to each other. The truck bearing the video camera and two lamps was almost balanced by a weight via pulley mechanism (not illustrated in Fig. 2) such that it could be held stationary at any location by virtue of friction unless pushed down or pulled up. The video-camera axis always remained horizontal and adjustable to intersect, at right angles, the central axis of the test section, the space confined by the electrodes in the test column. The two lamps were arranged symmetrically about the camera so that their optical axes lay on the same plane which included the camera axis and the central axis of the test section. The optical axis of each lamp intersected the camera axis at an angle of 12° on the central axis of the test section. This optical arrangement made it possible to picture each bouncing drop at its successive crossings of the central axis under the same optical condition so far as the truck, on which the camera-lamp assembly was mounted, moved in such a way that the camera axis followed the axial motion of the drop.

The operational range of the present experiments is defined in Table 1. Most of the experiments were carried out with drops 5.5 mm in D_0, the volume-equivalent spherical diameter, and with the electrode spacing adjusted at $l = 25$ mm, while the angle of tilt of the electrodes, θ, and the nominal electric field strength, $E_n(\equiv V/l)$, were varied from 0 to 73° and from 0.15 to 0.30 MV m^{-1}, respectively. In other experiments in which $D_0 = 3.7$ mm or $l = 40$ mm, θ was fixed at 45°.

2.2. Drop image processing

Drop images video-recorded with the experimental system described above were analyzed with the aid of the drop-image processing system constructed in our previous work [9]. Using the drop-image processing system, we measured the dimensions of each drop along its axes parallel and normal, respectively, to the electric field, D_p and D_n, and the position of its centroid at each instant. The processing of color of drop images was performed only with two frames, per round trip of each drop across the electrode spacing,

in which the images of the drop just crossing the midplane of the spacing were captured. For evaluating the color of each drop image, we cut out a small area covering 35×35 pixels about the geometrical center of the image to be processed. This size of area for color evaluation was determined such that the area never extended beyond the contour of any drop image obtained in the experiments.

The processing of sample areas, each covering 35×35 pixels, generally followed the scheme detailed in Nozaki et al. [9]. Following is an outline of the processing.

The successive frames registering a drop motion were stored in a Hi-8 video cassette recorder. Only the frames selected for the color-image processing were then sent to an image processor. The drop image captured in each of these frames was separated into R, G and B images, where R, G and B denote chromaticity coordinates. Each of these monochromatic images was digitized to 256 gradations, which were then spatially averaged over the sample area covering 35×35 pixels to evaluate the representative value on the relevant chromaticity coordinate. The R, G and B values thus evaluated for each frame were utilized in calculating the hue angle, H, and the saturation, S, as follows:

$$H=\tan^{-1}\left[\frac{\sqrt{3}(g-b)}{2r-g-b}\right]+H_0 \tag{1}$$

$$S=1-3\ \min\ (r,g,b) \tag{2}$$

where

$$r=\frac{R}{R+G+B}$$

$$g=\frac{G}{R+G+B} \tag{3}$$

$$b=\frac{B}{R+G+B}.$$

In the above, min (r, g, b) denotes the minimum of the three normalized chromaticity coordinates, r, g and b; and H_0 is defined as follows:

$$H_0=0\quad\text{for}\ \tan^{-1}\left[\frac{\sqrt{3}(g-b)}{2r-g-b}\right]\geq0$$

$$H_0=2\pi\quad\text{for}\ \tan^{-1}\left[\frac{\sqrt{3}(g-b)}{2r-g-b}\right]<0.$$

The calibration of H against drop temperature, T_d, was performed with an isothermal system adjusted at different temperatures step by step. The system consists of a silicone oil medium and isolated TLC-in-water suspension drop held together in a rectangular, water-jacketed PMMA cell. The cell is geometrically identical with the test column in a cross section normal to its axis but as short as 175 mm in axial length. Installed inside the cell are two brass plates, simulating the electrodes inside the test column, which are parallel to each other, leaving a 25-mm spacing between them, and they are also parallel to the cell axis. One brass plate at a higher position has a hole at its center, through which a black-colored 22-gauge stainless-steel needle is inserted vertically into the midportion of the spacing between the two brass plates. Manipulating a microsyringe to which the needle was connected, we could obtain a drop of desired size, 5.5 or 3.7 mm in D_0, pendant at the tip of the needle. The cell and the camera-lamp assembly were mounted on a rigid steel frame such that their geometrical arrangement well simulates the one used in heat-transfer experiments, and the drop in the cell was video-recorded under the same optical condition of arrangement for the heat-transfer experiments. The temperature in the cell was changed step by step such that H–T_d data were obtained at 18 different temperature levels distributed over a temperature range slightly exceeding the entire T_d range in the heat-transfer experiments. At each of 18 temperature levels, three different drops of each size were video-recorded for the purpose of confirming sufficient repeatability of H evaluation based on drop images. The set of H–T_d data thus obtained for each drop size was processed by a spline interpolation procedure incorporating algorithms of least-squares curve fitting [10] and of minimizing the sum of squares of residuals [11].

2.3. Drop-temperature data processing

The principle and the practical procedure of T_d-data processing for evaluating the characteristics of medium-to-drop heat transfer are outlined below. We suppose a drop released into the space between the electrodes in the test column. The energy balance for the drop may be written as

$$\frac{1}{6}\pi D_0^3\rho_d c_{pd}\frac{dT_{dm}}{dt}=\pi D_0^2\alpha(T_c-T_{dm}) \tag{4}$$

where ρ_d and c_{pd} are the mass density and the specific heat capacity, respectively, of the TLC-in-water suspension, T_{dm} is the mixed mean temperature of the drop, t is time, T_c is the undisturbed temperature of the surrounding silicone oil, α is the instantaneous, drop-surface-averaged, overall heat-transfer coefficient. The drop temperature, T_d, deduced from instantaneous H value must be deviating from T_{dm} more or less; pre-

sumably T_d is closer to the drop-surface temperature than to T_{dm}. The medium-to-drop heat flow rate represented by the right side of Eq. (4) may alternatively be given by $\pi D_0^2 \alpha'(T_c - T_d)$, where α' is a heat transfer coefficient presumably approximating the drop-surface-averaged, film heat transfer coefficient on the continuous-phase side. This leads to the following relation between the two definitions of medium-drop temperature difference:

$$T_c - T_{dm} = \frac{\alpha'}{\alpha}(T_c - T_d). \tag{5}$$

Substituting Eq. (5) into Eq. (4) and integrating it over a finite time lapse after some reference instant, $t = 0$, we obtain

$$-\ln\left(\frac{T_c - T_d}{T_c - T_{d,i}}\right) + \left[\ln\left(\frac{\alpha'}{\alpha}\right)\right]_{t=0} - \left[\ln\left(\frac{\alpha'}{\alpha}\right)\right]_{t=t} = \frac{6}{\rho_d c_{pd} D_0}\int_0^t \alpha \, dt \tag{6}$$

where the subscript i refers to the reference instant, $t = 0$. It is reasonable to assume that once the drop falls into a periodical bouncing motion across the electrode spacing, both α and α' (and hence α'/α) change periodically in synchronism with the motion of the drop. If the bouncing motion of the drop is already developed at the instant of $t = 0$ and the drop crosses the midplane of the space between the electrodes at each of the two instants, $t = 0$ and $t = t$, limiting the range of the above integral, the values of α'/α at those instants are considered to be the same. Hence, Eq. (6) becomes

$$-\ln\,(1 - F) = \frac{6}{\rho_d c_{pd} D_0}\int_0^t \alpha \, dt \tag{7}$$

where F is the temperature effectiveness for the dispersed phase, which is defined as

$$F = \frac{T_{dm} - T_{dm,i}}{T_c - T_{dm,i}} \tag{8}$$

and can be given by

$$F = \frac{T_d - T_{d,i}}{T_c - T_{d,i}} \tag{9}$$

on the condition that α'/α has the same values at the two instants, $t = 0$ and $t = t$. Differentiating Eq. (7) with x, the axial distance traveled by the drop after the reference instant, we have

$$-\frac{d}{dx}[\ln\,(1 - F)] = \frac{6}{\rho_d c_{pd} D_0}\frac{d}{dx}\int_0^t \alpha \, dt. \tag{10}$$

It should be noted here that we do not necessarily need to know α fluctuating at a high frequency in synchronism with the bouncing motion of the drop. What we generally need to know may be $\bar{\alpha}$, the overall heat transfer coefficient averaged over the period of one round trip of the drop between the electrodes. In converting α to $\bar{\alpha}$, T_d is assumed to be such an effectively continuous function of t or x as to connect smoothly the discrete T_d data obtained at successive crossings of the drop through the midplane of the spacing between the electrodes. In an axial region in which the bouncing motion of the drop is completely developed, $\bar{\alpha}$ as well as $\bar{v}_x$, the axial velocity of the drop averaged over one round trip of the drop, must be constant, and hence Eq. (10) becomes

$$-\frac{d}{dx}[\ln\,(1 - F)] = \frac{6\bar{\alpha}}{\rho_d c_{pd} D_0 \bar{v}_x}. \tag{11}$$

More than 50 sample drops were video-recorded, while making bouncing motions, at each operational condition characterized by a prescribed value of each of such parameters as D_0, l, E_n and θ. Selected from the records of all of the sample drops for each operational condition were those of 11 drops wherein we found a drop image laterally centered, with a good accuracy, in every frame. Further, drop images in which $S < 0.1$ (in the case $D_0 = 5.5$ mm) or $S < 0.085$ (in the case $D_0 = 3.7$ mm) were eliminated from those records. The residual drop images were then processed to obtain T_d data as well as the data on the trajectory of the center of each drop and also D_p and D_n of the drop. All of these data were then used to deduce $\bar{\alpha}$ data, which were then processed by a modified Tompson-τ algorithm [12] to eliminate extraordinary data. The $\bar{\alpha}$ data that had passed this statistical screening were used to calculate the mean value and the 95% coverage of $\bar{\alpha}$ under each operational condition.

The physical properties of the test liquids, water and a silicone oil, used in the above data-processing and the numerical predictions described later are summarized in Table 2. The property data given in the table are evaluated, otherwise noted, at temperature 51°C and are used as they are, neglecting their temperature dependencies.

3. Analytic model

Described below is a simple model for simulating the heat transfer to isolated drops each in a periodical bouncing motion in a space between paired electrodes. Our model for simulating such bouncing motions of drops, which was described elsewhere [5], is incorporated into the present model as the base for evaluating the continuous-phase-side thermal resistance.

Table 2
Physical properties of liquids used (at 51°C)

	ρ [kg m^{-3}]	ν [mm^2 s^{-1}]	c_p [kJ kg^{-1} K^{-1}]	λ [mW m^{-1} K^{-1}]	σ [mN m^{-1}]	ε [pF m^{-1}]	χ [Ωm]
Water	988[a]	0.553 (50°C)[b]	4.18[c]	640.5[c]		616[b]	5.3×10^4 (50°C)[a]
KF96 (10cSt)	902[d]	6.69[e]	1.465 (25°C)[f]	129.8 (25°C)[f]	44.6[g]	21.8[h]	4×10^{12}[h]

[a] Taken from Landolt–Börnstein Data Book [16].
[b] Taken from Malmberg and Maryott [17].
[c] Taken from Steam Tables [18].
[d] Measured with a pycnometer.
[e] Measured with a glass capillary viscometer.
[f] Manufacturer's data [19].
[g] Measured by the pendant drop method.
[h] Measured with the apparatus and procedure described by Kaji [20].

To be consistent with the model of drop motions [5], we assume each drop to be an electrically-conducting sphere suspended in a quiescent medium of a perfect dielectric liquid confined by a pair of tilted parallel-plate electrodes. The drop is subjected to the gravity, a Coulombic force, $\boldsymbol{F}_E$, and a hydrodynamic drag force, $\boldsymbol{F}_D$ (Fig. 3). The force balance on the drop is written just the same as in our previous paper reporting the drop-motion model [5]:

$$\frac{1}{6}\pi D^3\left(\rho_d+\frac{1}{2}\rho_c\right)\frac{d\boldsymbol{v}}{dt} = \frac{1}{6}\pi D^3(\rho_d-\rho_c)\boldsymbol{g}+\boldsymbol{F}_E-\boldsymbol{F}_D \tag{12}$$

where D is the diameter of the drop, ρ_d is the density of the drop, ρ_c is the density of the surrounding medium, $\boldsymbol{g}$ is the acceleration due to gravity, and $\boldsymbol{v}$ is the instantaneous velocity of the drop. The inertia force term on the left-hand-side of Eq. (12) includes the virtual mass of the drop, which is approximated by that of a rigid sphere, volume-equivalent to the drop, in a steady translation through an inviscid fluid medium of an infinite extent. $\boldsymbol{F}_D$ is expressed as

$$\boldsymbol{F}_D=\frac{1}{8}\pi\rho_c C_D D^2\,|\,\boldsymbol{v}\,|\,\boldsymbol{v} \tag{13}$$

where C_D is the drag coefficient that a sphere volume-equivalent to the drop would have if it moved at a constant speed $|\boldsymbol{v}|$. In our former study [5], we expressed the relation between C_D and the Reynolds number, $Re\equiv|\boldsymbol{v}|D/\nu_c$ (where ν_c is the kinematic viscosity of the surrounding medium), by use of a multisegment correlation recommended by Clift et al. [13]. This time we employ Turton and Levenspiel's correlation [14] which is much simpler and slightly better in accuracy:

$$C_D=\frac{24}{Re}(1+0.173Re^{0.657})+\frac{0.413}{1+16300Re^{-1.09}}. \tag{14}$$

The Coulombic force $\boldsymbol{F}_E$ is defined to be positive when it is in the direction of an increasing voltage, and its magnitude is evaluated as

$$|\,\boldsymbol{F}_E\,|=|\,Q\,|\,E_n \tag{15}$$

where Q is the net charge on the drop, which is approximated by the charge that a rigid conducting sphere of diameter D would have when in contact with a conducting plate used as either electrode. According to Félici [15], the magnitude of Q is given by

$$|\,Q\,|=\frac{1}{6}\pi^3\varepsilon_c D^2 E_n \tag{16}$$

where ε_c is the electrical permittivity of the surrounding medium.

To solve the above set of equations for $x(t)$, $y(t)$ and $\boldsymbol{v}(t)$, we need to specify the mechanical condition

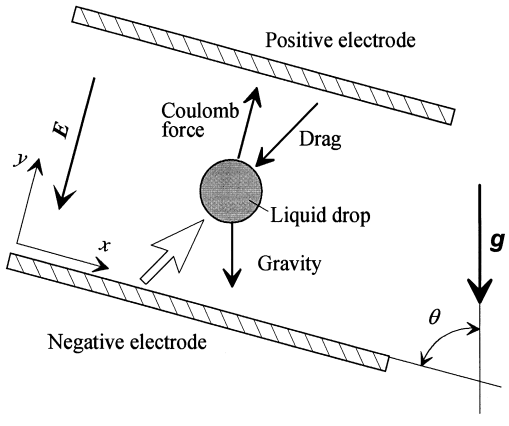

Fig. 3. Forces acting on a drop obliquely crossing the space between parallel plate electrodes. The x–y coordinates are laid on the surface of the electrode at a lower position such that the x-axis coincides with the longitudinal direction of the electrodes.

of drop-electrode collisions. In our previous study [5], we found that the bouncing motions of water drops in a silicone oil medium were predicted most accurately by the rigid conducting-sphere model when it incorporated the 'stick condition'—a model of the drop-electrode collisions which assumes that at each collision with electrode surface, a drop completely loses its momentum and 'sticks' on the surface before leaving there in a moment. Thus, we employ the 'stick condition' approximation together with Eqs. (13)–(16) in the process of integrating Eq. (12), thereby deducing $x(t)$, $y(t)$ and $\boldsymbol{v}(t)$ for each drop.

Once the motion of a drop is calculated, we can estimate α, the instantaneous, overall heat transfer coefficient, on the assumption that the overall thermal resistance, $1/\alpha$, is given by simply summing $1/\alpha_c$, the external resistance around an isothermal sphere which is volume-equivalent with the drop and is translating just the same as the drop, and $1/\alpha_d$, the internal resistance of sphere. This assumption may be expressed as

$$\frac{1}{Nu} = \frac{1}{Nu_c} + \frac{\lambda_c}{\lambda_d}\frac{1}{Nu_d} \tag{17}$$

where λ_c and λ_d are the thermal conductivities of the continuous-phase liquid and the dispersed-phase liquid, respectively, and the three Nusselt numbers are defined as $Nu \equiv \alpha D/\lambda_c$, $Nu_c \equiv \alpha_c D/\lambda_c$ and $Nu_d \equiv \alpha_d D/\lambda_d$. For evaluating Nu_c, we assume the instantaneous, continuous-phase-side heat transfer to be quasi-steady and predictable by the following multisegment correlation for the steady heat transfer to/from the isothermal surface of a rigid sphere (Clift et al. [13]):

$$Nu_c = 1 + (1 + Pe)^{1/3} \quad (Re \le 1)$$

$$Nu_c = \left(1 + \frac{1}{Pe}\right)^{1/3} Re^{0.41}\, Pr^{1/3} + 1 \quad (1 < Re \le 100) \tag{18}$$

$$Nu_c = 0.752 Re^{0.472}\, Pr^{1/3} \left(1 + \frac{1}{Pe}\right)^{1/3} + 1 \quad (100 < Re \le 2000)$$

where Pr is the Prandtl number of the continuous-phase liquid and Pe is the Péclét number defined as $Pe \equiv Re\ Pr$. As for Nu_d, we employ two extreme evaluations for alternative use: one is the Newman solution for the asymptotic stage of transient conductive heat transfer inside a rigid sphere, $Nu_d = 6.58$, and the other is $Nu_d \to \infty$ which should result from the complete mixing inside the drop. The experimental observations show that each drop is appreciably squeezed at each impact with an electrode and then exhibits a damped shape-oscillation while leaving away from the electrode. The effective value of Nu_d in such oscillating drops should be intermediate between the above-referenced extreme values.

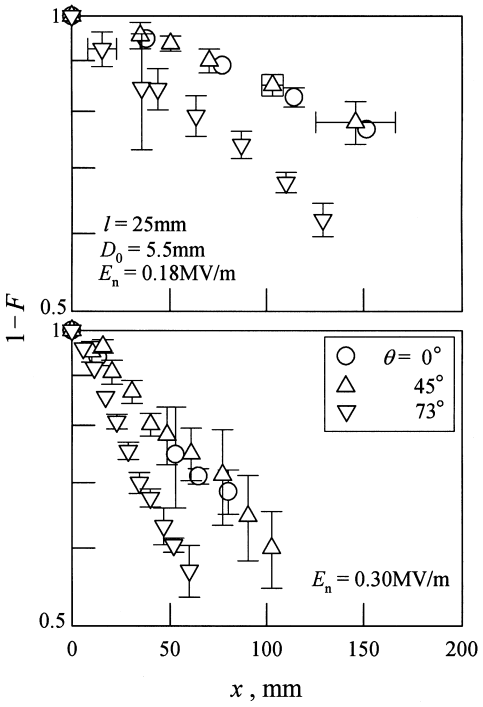

Fig. 4. Axial variations of the component of F, the temperature effectiveness for drops given by Eq. (9), at three orientations of the electrodes. Each symbol indicates the mean of (F, x) data obtained in more than several runs in each of which the axial passage of a drop was followed by a video camera. The origin of x-axis is defined as the axial location where each drop crosses the midplane of the electrode spacing, giving its first image satisfying the condition that $S \geqslant 0.1$. Thus, the location of $x = 0$ in the test section may differ from run to run. Each error bar attached to a symbol represents the uncertainty of 95% coverage, in $1-F$ or in x, about the relevant mean value indicated by the symbol. No error bar is attached to a symbol when the relevant uncertainty is less than the coordinate span covered by the symbol itself.

The instantaneous, overall heat transfer coefficient α thus evaluated is then used to calculate $\bar{\alpha}$, the overall heat transfer coefficient averaged over one round trip of the drop between the electrodes as

$$\frac{\bar{\alpha}\Lambda_x}{\bar{v}_x} = \int_t^{t+\tau} \alpha\, \mathrm{d}t \tag{19}$$

where Λ_x is the axial displacement of the drop during one round trip and τ is the time lapse during the trip. The values of $\bar{\alpha}$ predicted in this way will be compared with relevant experimental values in the subsequent section.

Table 3
Heat transfer coefficients, α, for water drops steadily falling due to gravity in the absence of electric field—comparison of experimental and predicted values

	α [W m^{-2} K^{-2}]		
		Predicted	
D_0 [mm]	Experimental	Asymptotic internal conduction ($Nu_d = 6.58$)	Complete internal mixing ($Nu_d = \infty$)
3.7	$1.58\times10^2\pm7.52$	3.80×10^2	5.67×10^2
5.5	$1.98\times10^2\pm30.8$	3.12×10^2	5.26×10^2

4. Results and discussions

Fig. 4 exemplifies experimentally obtained axial variations of F, the temperature effectiveness for drops, at three different orientations of the electrodes under each of the two different levels of electric field strength. To examine their consistency with the F–$\bar{\alpha}$ relation indicated by Eq. (11), the $F(x)$ data are plotted in a semi-logarithmic $(1-F)$ vs. x diagram. The data for each operational condition are aligned almost linear, indicating that $\bar{\alpha}$ is held nearly constant throughout the axial passage of drops under a given condition. Also known from Fig. 4 is an effectiveness of simultaneously increasing E_n and θ for obtaining high F values at short axial passages of drops.

In order to evaluate the accuracy of deducing $\bar{\alpha}$ from the TLC-thermometrically obtained T_d data via Eq. (11), this $\bar{\alpha}$-deducing procedure was first tested with water drops simply falling in the silicone oil due to gravity only ($E_n = 0$). The heat transfer in this situation was intrinsically quasi-steady so that there is no need to discriminate between $\bar{\alpha}$ and α. The values of α deduced by the above procedure are listed in Table 3 for comparison with the corresponding predictions of α based on the rigid sphere model described in Section 3. Here we unexpectedly find that the T_d-data-based experimental α values are even lower than the corresponding predictions based on the assumption of the asymptotic stage of conductive heat transfer inside drops. This fact is unaccountable unless we assume some change in $(T_c - T_{dm})/(T_c - T_d)$ with time for each falling drop, resulting in a failure of the assumption of constant α'/α. The TLC microcapsules initially well mixed in each drop were presumably sedimented toward the bottom portion of the drop with the lapse of time, thereby yielding a tendency of an increasing deviation of TLC-thermometrically determined T_d from the drop-surface temperature. This tendency should have resulted in an apparent decrease in the rate of increase in F, the temperature effectiveness calculated by Eq. (9), and hence an underestimation of α. The underestimation of α due to the above mechanism must have been reduced for drops making bouncing motions between the electrodes because of a periodical internal mixing caused by the shape oscillations that the drops underwent as the result of their successive collisions with the electrodes. Nevertheless, we still need to take account of some, though not significant, underestimation of $\bar{\alpha}$ for drops making bouncing motions, particularly for those subjected to rather weak electric fields (typically $E_n \lesssim 0.2$ MV m^{-1}), as discussed later.

Figs. 5–8 show the variations of $\bar{\alpha}$ with operational parameters—E_n, θ, l and D_0. Compared in each diagram are the experimental results based on the TLC-thermometry and Eq. (11) and the predictions incor-

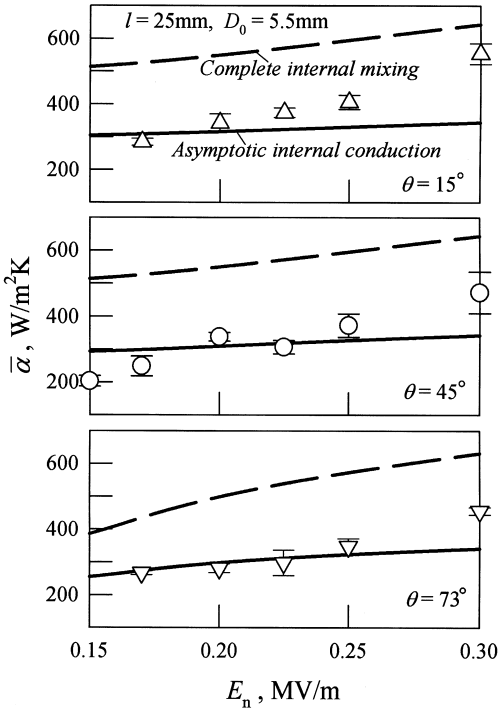

Fig. 5. Dependencies of the time-averaged, overall heat transfer coefficient, $\bar{\alpha}$, on the electric field strength averaged over the electrode spacing, E_n.

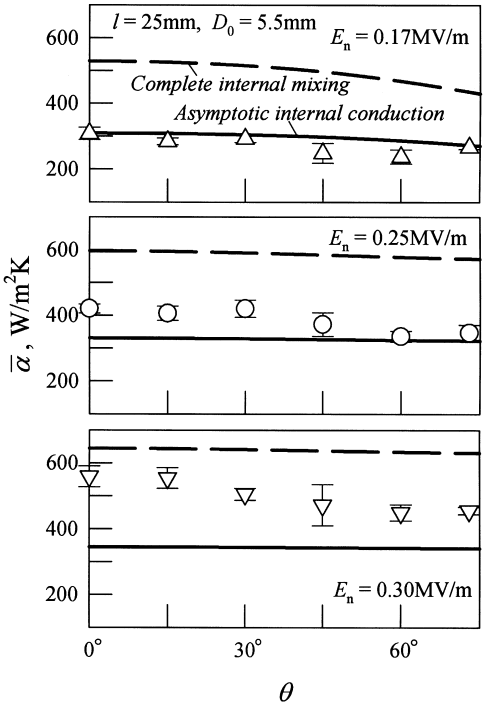

Fig. 6. Dependencies of the time-averaged, overall heat transfer coefficient, $\bar{\alpha}$, on the angle of tilt of the electrodes, θ.

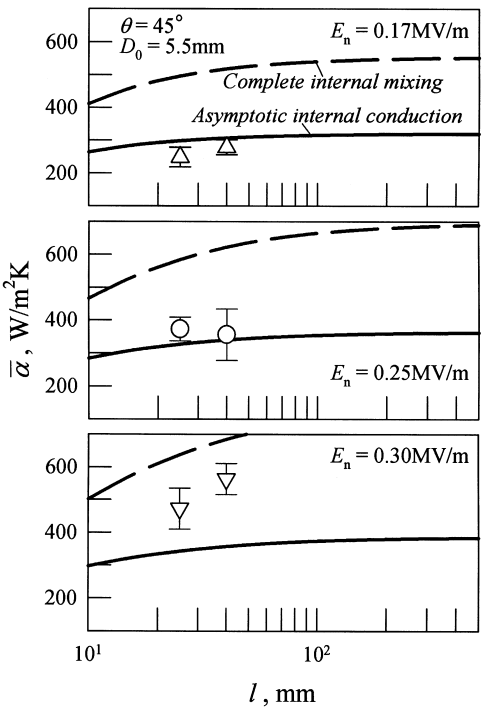

Fig. 7. Dependencies of the time-averaged, overall heat transfer coefficient, $\bar{\alpha}$, on the electrode spacing, l.

porating the two extreme assumptions, $Nu_d = 6.58$ and $Nu_d = \infty$, for alternative use.

Fig. 5 shows the dependencies of $\bar{\alpha}$ on E_n at three different angles of tilt of the electrodes, while the other parameters, l and D_0, are fixed. Some of the experimental points in the range $E_n \leq 0.225$ MV m^{-1} indicate $\bar{\alpha}$ values lower than the predictions related to the assumption that $Nu_d = 6.58$, thereby suggesting some residual effect of the sedimentation of the TLC microcapsules inside the drops making not-too-intensive bouncing motions. On the other hand, the experimental points tend to exceed those minimum predictions and to show $\bar{\alpha}$ values intermediate between the two classes of the predictions with an increase in E_n beyond some 0.25 MV m^{-1}. The shape oscillation of drops generated by their collisions with the electrodes is presumably the primary cause of such an increase in $\bar{\alpha}$.

Fig. 6 shows the dependencies of $\bar{\alpha}$ on θ at three different field strengths. Again we find the experimental $\bar{\alpha}$ values below the corresponding minimum predictions irrespective of θ at the weakest field strength, E_n = 0.175 MV m^{-1}, which is ascribable to the internal sedimentation of TLC microcapsules. What should be noted in Fig. 6 is that the theoretical predictions represent that the tendency of a decreasing $\bar{\alpha}$ with an increasing θ becomes weaker with an increase in E_n. This is a consequence of the fact, confirmed both experimentally and numerically, that $\bar{v}_t$, the time-averaged translational velocity of each drop, decreases with an increase in θ considerably at lower E_ns but only slightly at higher E_n's [5]. In contrast with such predictions, the experimental results show that the decrease in $\bar{\alpha}$ with an increasing θ becomes even sharper with an increase in E_n. This inconsistency between the predictions and the experimental finding is presumably ascribable to the neglect of the effect of thermal wakes formed behind drops in the analytic model described in Section 3. The trajectory of each drop becomes more closely zigzagged, excessively shortening Λ_x, with an increase in θ particularly when E_n is high. As Λ_x/l significantly decreases, each drop inevitably interacts with its own wake when it rebounds from either electrode. In fact, the major proportion of the surface of the drop may be enveloped in the wake in an early part of each drop's crossing of the electrode spacing when Λ_x/l is substantially lower than unity. The increasing extent of the drop-wake interaction with an increase in θ is presumed to be the primary cause of the decrease in $\bar{\alpha}$ with an increase in θ at higher levels of E_n.

Fig. 7 gives an $\bar{\alpha}$ vs. l diagram. Since only two different l values were employed in the experiments, it is difficult to know the l dependency of $\bar{\alpha}$ at each level of E_n from the experimental results. The numerical predictions reveal a tendency that $\bar{\alpha}$ gradually increases with

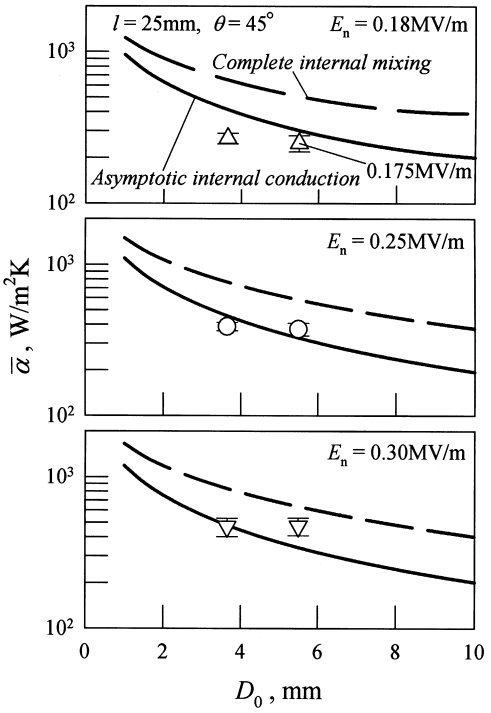

Fig. 8. Dependencies of the time-averaged, overall heat transfer coefficient, $\bar{\alpha}$, on the drop diameter, D_0.

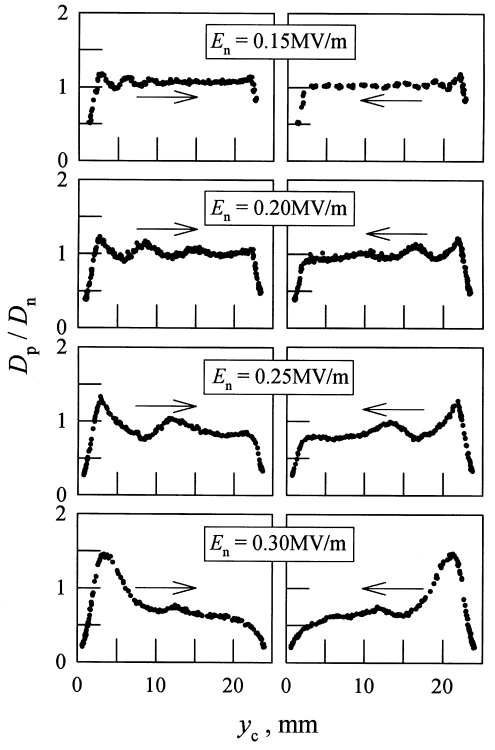

Fig. 9. Variations of distortion ratio of drops during their crossings of the electrode spacing. Each dot indicates D_p/D_n of a drop and y_c, the y-axial distance measured from the surface of the negative electrode to the center of the drop, at an instant. A chain of dots in each D_p/D_n–y_c diagram represents the shape-location record of a drop while it was crossing the electrode spacing in the direction indicated by the arrow illustrated at the side of the dots. $l = 25$ mm, $D_0 = 4.9$ mm, $\theta = 45°$.

an increase in l, which results from the nature of $\bar{v}_t$ increasing, with an increasing l, asymptotically toward the steady velocity prescribed by E_n and θ. Another advantage of an increasing l lies, though not experimentally confirmed, in that it should relatively reduce the unfavorable effect of drop–wake interaction. It turns out, however, that an increase in l is generally accompanied with a significant drawback, once we consider a multi-drop system, instead of a single drop system, confined in a heat exchanger. The maximum holdup ratio allowed for stable operation of the exchanger should decrease [6,7], with an increase in l, thereby decreasing the limit of the volumetric heat transfer coefficient in the exchanger [8].

In Fig. 8, $\bar{\alpha}$ is plotted against D_0. The numerical predictions indicate a monotonic decrease of $\bar{\alpha}$ with an increase in D_0. However, we find no appreciable difference between $\bar{\alpha}$ values experimentally obtained with smaller ($D_0 = 3.7$ mm) and larger ($D_0 = 5.5$ mm) drops, respectively. The shape oscillation was less intensive with smaller drops, and hence the underestimation of $\bar{\alpha}$ due to the sedimentation of TLC microcapsules must be more significant with the smaller drops. This is presumably the reason why we find no D_0 dependency in the experimental results.

Finally we discuss two matters which possibly affected the experimental results shown above but are not taken into account in the analytic model: they are the shape oscillation (or, more appropriately, oscillatory deformation) of drops and the heat conduction from the electrodes to drops while they are in mutual contact with each other. These two matters are examined in order.

Fig. 9 exemplifies the variations in the distortion ratio of drops during their crossing of the electrode spacing, which were identified in our previous 16-mm film records of drops in motion [5]. It is generally recognized that each drop is considerably flattened when it collides with an electrode, then springs into an oblate-to-prolate deformation, and successively falls into a rather asymptotic deformation process, accompanied with some fluctuation, which continues until the drop comes close to the opposite electrode. Under a weak electric field ($E_n \leq 0.20$ MV m^{-1}), the distortion of a drop is held nearly constant throughout its crossing of the bulk of the electrode spacing. As E_n is raised further, the distortion of each drop exhibits a significant wriggling during its passage through the

electrode spacing. The above observation is consistent with the presumption of the sedimentation of TLC microcapsules inside drops under weak electric fields and also with the tendency of experimental $\bar{\alpha}$ values exceeding the corresponding $\bar{\alpha}$ predictions based on the assumption of no mixing inside drops.

The electrodes are considered to be held at nearly the same temperature as that of the medium liquid. Thus, it is reasonable to assume that heat is conducted from each electrode to each drop during their mutual contact. The amount of heat flowing into the drop during each contact period is estimated by numerically analyzing the transient, conductive heat transfer across the electrode, a thin silicone oil film between the electrode and the drop, and the drop itself. The details of the analysis are given in the Appendix. The conclusion of the analysis is that the amount of heat conducted from the electrodes into the drop during two contact periods in one round trip of the drop across the electrode spacing is at most 13% of the total amount of heat transferred to the drop in every round trip on condition that D_0 is some 5 mm and $E_n = 0.3$ MV m^{-1}. Thus, it may be said that the conductive heat transfer from the electrodes may not be negligible but not so significant as to be incorporated into the model presented in this paper, considering its highly approximate nature.

5. Conclusions

The heat transfer to single liquid drops exhibiting periodical bouncing motions across a liquid-filled space between parallel-plate electrodes has been studied both experimentally and numerically. The TLC-microcapsule thermometry recently developed was applied to continuously detect the temperature change in each traveling drop in order to deduce the instantaneous temperature effectiveness of the drop and the overall medium-to-drop heat transfer coefficient. This experimental technique was found to be useful when the drops are accompanied with significant shape oscillation which causes an internal mixing, thereby allowing the TLC microcapsules to remain well dispersed inside the drops. In the absence of effective internal mixing, an inevitable sedimentation of TLC microcapsules inside drops may lead to a misevaluation of the heat transfer coefficient.

Despite the above-mentioned technical difficulties involved in the experiments, the results obtained in the experiments have clarified the general dependencies of the medium-to-drop heat transfer on major operational parameters. As expected, simultaneous increases in the electric field strength and the angle of tilt of the electrodes are found to be quite effective to attain a sufficiently high temperature effectiveness for drops within a short axial distance traveled by the drops. The results also indicate that the shape oscillation excited on each drop at its every collision with either electrode may considerably enhance the heat transfer.

An analytic model regarding drops as rigid spheres has been formulated such that the instantaneous heat transfer to each drop can be numerically simulated. Despite extensive simplifications involved in it, the model predicts the characteristics of the heat transfer with a reasonable accuracy. This fact suggests a potential utility of the model as a tool for designing a novel type of liquid–liquid contactors (direct contact heat exchangers or liquid–liquid extractors) each incorporating the device of tilted parallel-plate electrodes in it.

Acknowledgements

We would like to thank A. Taniguchi, T. Yamamoto and Y. Hoshino, former students at Keio University, for their assistance carrying out the experiments and the work of drop-image analysis. We are also indebted to K. Nogami, K. Sakai and T. Utsumi, former and present students at the Polytechnic University, for their help in the image-analysis work.

Appendix. Evaluation of conductive heat transfer from electrodes to drops

Drops each making bouncing motion between the positive and the negative electrodes collide once with respective electrodes in a 'round trans-electrode spacing trip'. At each collision of the drop with either electrode, some amount of heat is possibly transferred into the drop from the electrode which is otherwise nearly in thermal equilibrium with the medium liquid. Described below is an attempt to roughly evaluate the relative contribution of the above heat-flow route to the overall heat transfer to the drop.

High-speed cinephotographic drop-motion records obtained in our experiments reported in Ref. [5] show that when each water drop, $D_0 \approx 5$ mm, approaches an electrode within $\sim$1 mm, it already has a nearly planar front laterally extending to a substantial proportion of its projection normal to the electrode. The silicone oil intervening between the drop front and the electrode surface must be radially drained as the drop is being pressed against the electrode surface by some net force. The transient, conductive heat transfer from the electrode to the drop across the intervening silicone oil layer during the period of such drop-to-electrode interaction is analyzed, introducing the following assumptions:

1. the drop has a planar, circular front so that the

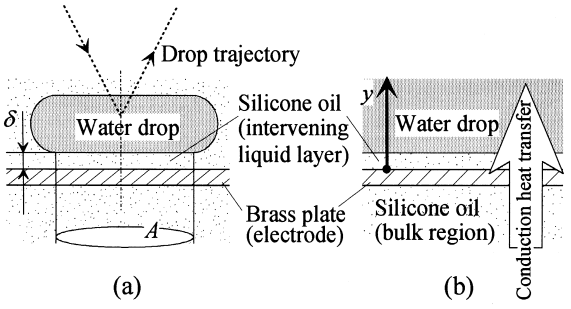

Fig. A1. Drop-to-electrode interaction. (a) Schematic of a water drop having approached the negative electrode. (b) Modeling of one-dimensional heat conduction to the drop across a series composite layer.

intervening silicone oil layer is uniform in thickness over an area A at each instant (see Fig. A1(a));
2. the thickness of the silicone oil layer, δ, is so small that we can safely use the usual lubrication approximation in describing the radial, squeezing flow in the layer;
3. the front of the drop is tangentially immobile so that a no-slip condition may be imposed on both boundaries of the silicone oil layer; and
4. the electrode is backed by a stationary silicone oil phase having a semi-infinite extent (Fig. A1(b)).

Using assumptions (1)–(3), we can derive the following expression for the rate of change of the thickness of the intervening silicone oil layer [21]:

$$-\frac{\mathrm{d}\delta}{\mathrm{d}t}=\frac{8\pi\delta^3\rho_c F_I}{3\nu_c A^2} \tag{A1}$$

where F_I is the spatial integral of the static pressure in the silicone oil layer over the area A. If we assume the depletion of silicone oil beneath the drop to be a quasi-steady process, we can integrate Eq. (A1) as

$$\frac{1}{2}(\delta^{-2}-\delta_0^{-2})=\frac{8\pi\rho_c}{3\nu_c}\int_{t_0}^{t}\frac{F_I}{A^2}\,\mathrm{d}t \tag{A2}$$

where t_0 denotes the moment of emergence of a flat drop front, and δ_0 is the thickness of the silicone oil layer still left between the drop front and the electrode surface at the moment $t=t_0$. At each instant, F_I must be in balance with the component, normal to the electrode surface, of the resultant of the external forces acting on the drop. Thus, it turns out that for a silicone oil layer on the negative electrode,

$$\boldsymbol{F}_I=\pm\mid Q\mid E_n+\frac{1}{6}\pi D_0^3\frac{\mathrm{d}^2y_c}{\mathrm{d}t^2}\left(\rho_d+\frac{1}{2}\rho_c\right)-\frac{1}{6}\pi D_0^3\quad(\rho_c-\rho_d)\mid\boldsymbol{g}\mid\ \cos\ \theta \tag{A3.1}$$

and for the one on the positive electrode,

$$\boldsymbol{F}_I=\pm\mid Q\mid E_n-\frac{1}{6}\pi D_0^3\frac{\mathrm{d}^2y_c}{\mathrm{d}t^2}\left(\rho_d+\frac{1}{2}\rho_c\right)+\frac{1}{6}\pi D_0^3\quad(\rho_c-\rho_d)\mid\boldsymbol{g}\mid\ \cos\ \theta \tag{A3.2}$$

where y_c is the y-axial location of the center of the drop. The positive sign leading the first term on the right-hand-side refers to a δ range that $\delta\geq\delta_c$, while the minus sign refers to the range $\delta<\delta_c$, where δ_c is the silicone-oil-layer thickness critical for a dielectric breakdown across the layer. It is assumed that the breakdown occurs when δ decrease to δ_c, immediately exchanging the charge on the drop.

Since water drops are much more conducting than the silicone oil, it is reasonable to assume that each drop approaching either electrode has an equipotential surface. The potential at the surface of the drop must be nearly the same as that at the other electrode with which the drop made the last electrical contact. Therefore, we can evaluate δ_c on the assumption that $|V|/\delta_c$ gives the electric strength of the silicone oil. Consulting the literature for the general dependency of electric strengths of liquids on electrode spacing [22] and manufacturer's data on the electric strength of the silicone oil [19], we have prepared the following correlation for use in evaluatingδ_c:

$$\frac{\delta_c}{[\mathrm{m}]}\Big/\frac{|V|}{[\mathrm{MV}]}=0.02016\ \ln\left(\frac{\delta_c}{[\mathrm{m}]}\right)+0.1922. \tag{A4}$$

Analyzing our previous high-speed cinephotographic records of drops in motion [5], we can obtain data on the variations in y_c and A during the periods of apparent drop-to-electrode interactions. We have collected such $y_c(t)$ and $A(t)$ data in the sequences of seven successive collisions of a drop with each electrode, where t is defined as the time lapse after y_c (or $l-y_c$) takes the minimum value during each collision of the drop with the negative (or the positive) electrode. Exemplified in diagrams (a) and (b) in Fig. A2 are such collected data for the collisions with the negative electrode. The data are well aligned, indicating a good repeatability of the drop-to-electrode collisions. A spline curve interpolation procedure was applied to those discrete data to derive continuous y_c–t and A–t relations which are indicated by solid curves in diagrams (a) and (b), respectively. Evaluating F_I in Eqs. (A3.1) or (A3.2) with the aid of the y_c–t relation and Eq. (A4), and then substituting the resultant F_I–t relation, together with the A–t relation, into Eq. (A2) to perform the integration

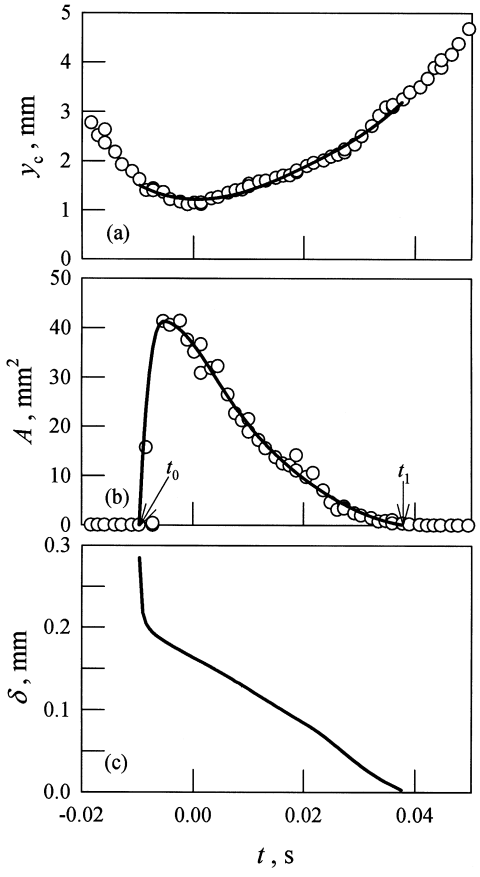

Fig. A2. Variations in y-axial location of drop center (a), planar drop-to-electrode contact area (b), and the thickness of silicone oil layer between drop and electrode (c) during collision of a water drop with negative electrode. $l = 25$ mm, $D_0 = 4.9$ mm, $\theta = 45°$, $E_n = 0.32$ MV m^{-1}. The data indicated by open circles are obtained in seven successive collisions of a drop with the same negative electrode and plotted against time axis, t, whose origin, $t = 0$, is defined as the instant of the minimum y_c for each collision. The solid curves in (a) and (b) are drawn by a spline curve-fitting procedure. The curve in (c) is calculated using Eqs. (A2), (A3.1) and (A4).

on the right-hand-side, we can calculate δ varying with t. Diagram (c) in Fig. A2 shows the δ–t relation relevant to the y_c–t and A–t relations given in diagrams (a) and (b), respectively.

The A–t and δ–t relations thus obtained are utilized in calculating the conductive heat transfer to each drop through the planar contact area A. This heat transfer process is regarded as a transient, one-dimensional conduction across a series composite layer. As illustrated in Fig. A1(b), the layer farthest from the drop is a bulk silicone oil phase extending to $y = -\infty$ or $y = \infty$. The second layer is a brass plate used as an electrode. The third one is the intervening silicone oil with variable thickness δ. The drop itself is regarded as a semi-infinite water layer occupying the space $\delta \le y \le \infty$ or $-\infty \le y \le l - \delta$. The heat diffusion equation is written as

$$\rho_j c_{pj} \frac{\partial T}{\partial t} = \frac{\partial}{\partial y}\left(\lambda_j \frac{\partial T}{\partial y}\right) \tag{A5}$$

where the subscript j refers to each of the four layers specified above. The initial and the boundary conditions we employ are as follows:

$$\begin{aligned} t = t_0: \quad & T = T_c \quad (y < \delta \text{ or } y > l - \delta) \\ & T = T_{d0} \quad (y \ge \delta \text{ or } y \le l - \delta) \end{aligned} \tag{A6}$$

$$\begin{aligned} & y < -\delta_e \quad \text{or} \quad l + \delta_e < y: \quad \rho_j = \rho_c, \quad c_{pj} = c_{pc}, \quad \lambda_j = \lambda_c \\ & -\delta_e \le y < 0 \quad \text{or} \quad l < y \le l + \delta_e: \quad \rho_j = \rho_b, \quad c_{pj} = c_{pb}, \\ & \lambda_j = \lambda_b \\ & 0 \le y < \delta \quad \text{or} \quad l - \delta < y \le l: \quad \rho_j = \rho_c, \quad c_{pj} = c_{pc}, \quad \lambda_j = \lambda_c \\ & \delta \le y \quad \text{or} \quad y \le l - \delta: \quad \rho_j = \rho_d, \quad c_{pj} = c_{pd}, \\ & \lambda_j = \lambda_d \end{aligned} \tag{A7}$$

where δ_e is the thickness of the electrode plate, and the subscript b refers to brass. A finite difference scheme is used to integrate Eq. (A5) under the conditions given in Eqs. (A6) and (A7). In doing so, the interval of nodal-points, Δy, is set at 0.5 mm throughout the silicone oil layer behind the electrode, the electrode and the water layer, while Δy in the intervening silicone oil layer is set at one-twentieth of δ, the thickness of the layer. The time increment, Δt, relevant to the integration of the left-hand-side of Eq. (A5), is so adjusted as to satisfy the following requirement for computational stability:

$$\Delta t < \text{minimum value of } (\rho_c c_{pc} \Delta y / 2\lambda_c) \tag{A8}$$

where $\Delta y = \delta/20$. Integrating Eq. (A5) with the aid of Eqs. (A6)–(A8), we can calculate, for each instant, the temperature profile along y-axis (as exemplified in Fig. A3) and the heat flux at the silicone-oil/water interface, q, given by

$$q = -\lambda_d \frac{\partial T}{\partial y} \quad \text{or} \quad \lambda_d \left.\frac{\partial T}{\partial y}\right|_{y = l - \delta} \tag{A9}$$

where the temperature gradient is to be evaluated at the water-side of the interface. The total amount of

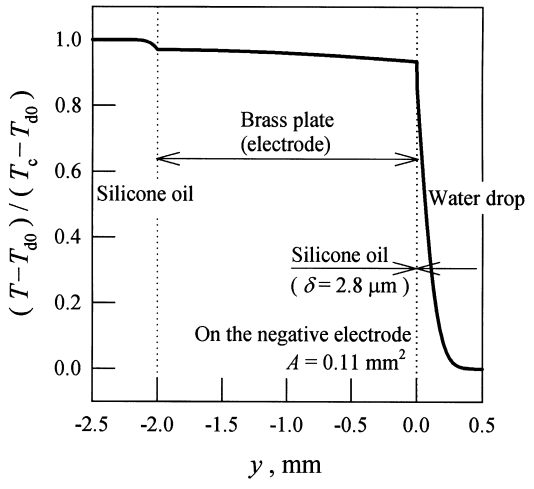

Fig. A3. Temperature profile at a moment when a drop is just leaving from negative electrode. This profile corresponds to the time $t=0.0376$ s in diagrams shown in Fig. A2. A silicone oil film, 2.8 μm in thickness, intervenes between the electrode and the water drop at this instant.

heat Q_t transferred into the drop through the drop-to-electrode contact area, A, during the period of each collision, $t_0 \le t \le t_1$, is evaluated as

$$Q_t = \int_{t_0}^{t_1} Aq \, dt \tag{A10}$$

where t_0 and t_1 are identified as the instants at which the area A emerges, followed by a sharp expansion, and vanishes, respectively (see diagram (b) in Fig. A2).

It should be noted that each drop experiences one collision with the negative electrode and one with the positive electrode during its one round trip across the electrode spacing. We need to estimate the sum of Q_ts for these two collisions, which is to be compared with the total heat actually transferred to the drop during its one round trip including those two collisions. The 'initial' drop temperature, T_{d0}, for the latter collision, one with positive electrode, must be higher than that for the former collision, the other with negative electrode. However, the change in T_{d0} between those collisions is neglected in our estimation of the sum of Q_ts, because it is not substantial compared to the magnitude of $T_c - T_{d0}$.

In a typical operational condition of $l=25$ mm, $D_0=4.9$ mm, $\theta=45^\circ$ and $E_n=0.30$ MV m^{-1}, for example, the sum of Q_ts for two successive collisions of a drop with the electrodes is calculated to be about 13% of the corresponding experimental value of the total heat transferred to the drop during its one round trip. The relative contribution of the electrode-to-drop conductive heat transfer possibly increases with a decrease in l and an increase in D_0.

References

[1] Y.H. Mori, N. Kaji, An augmentation method of heat or mass transfer between drops and a medium by the application of an electric field. Japanese Patent No. 1 335 398 (1986).

[2] N. Kaji, Y.H. Mori, Y. Tochitani, K. Komotori, Electrohydrodynamic augmentation of direct-contact heat transfer to drops passing through an immiscible dielectric liquid: effects of field-induced shuttle migration between parallel plane electrodes of drops, in: Proceedings of the 7th International Heat Transfer Conference, vol. 5, Hemisphere, Washington, DC, 1982, pp. 231–236.

[3] T. Mochizuki, Y.H. Mori, N. Kaji, Augmentation of direct-contact heat transfer to a train of drops through application of a transverse electric field, Journal of Chemical Engineering of Japan 20 (1987) 608–613.

[4] N. Kaji, Y.H. Mori, Bouncing motion of drops and particles between parallel-plate electrodes—a preliminary study of drying augmentation, in: A.S. Mujumdar (Ed.), Drying '86, Hemisphere, Washington, DC, 1986, pp. 819–827.

[5] T. Mochizuki, Y.H. Mori, N. Kaji, Bouncing motions of liquid drops between tilted parallel-plate electrodes, AIChE Journal 36 (1990) 1039–1045.

[6] T. Mochizuki, Y.H. Mori, N. Kaji, Drop interactions in electrostatic liquid–liquid contactors, AIChE Journal 38 (1992) 311–314.

[7] T. Mochizuki, Y.H. Mori, N. Kaji, Drop interactions in electric fields across tilted parallel-plate electrodes, JSME International Journal, Series B 36 (1993) 628–635.

[8] T. Mochizuki, Y.H. Mori, A novel design of liquid–liquid contactors with an electrical enhancement device—a simulation of their performance, in: D.M. Maron (Ed.), Proceedings of International Symposium on Liquid–Liquid Two-Phase Flow and Transport Phenomena, Begell House, Inc, New York, 1998, pp. 583–594.

[9] T. Nozaki, T. Mochizuki, N. Kaji, Y.H. Mori, Application of liquid–crystal thermometry to drop temperature measurements, Experiments in Fluids 18 (1995) 137–144.

[10] K. Ichida, F. Yoshimoto, Spline Functions and Their Applications (in Japanese), Kyoikushuppan, Tokyo, 1988.

[11] K. Ichida, F. Yoshimoto, T. Kiyono, Curve fitting by a piecewise cubic polynomial, Computing 16 (1976) 329–338.

[12] ASME Measurement Uncertainty—ANSI/ASME PTC 19.1-1985, Performance Test Codes, Supplement on Instruments and Apparatus, Part 1 1986.

[13] R. Clift, J.R. Grace, M.E. Weber, Bubbles, Drops, and Particles, Academic Press, New York, 1978, pp. 30–60, 121–123, 130–137.

[14] R. Turton, O. Levenspiel, A short note on the drag cor-

relation for spheres, Powder Technology 47 (1986) 83–86.
[15] N-J. Félici, Forces et charges de petits objets en contact avec une électrode affectée d'un champ électrique, Revue Générale de L'Électricité 75 (1966) 1145–1160.
[16] Landolt–Börnstein Zahlenwerte und Funktionen aus Physik, Chemie, Astronomie, Geophysik und Technik, II-6, II-7 and IV-1. Springer-Verlag, Berlin, 1955, 1959, 1960.
[17] C.G. Malmberg, A.A. Maryott, Dielectric constant of water from 0° to 100°C, Journal of Research of the National Bureau of Standards 56 (1956) 1–8.
[18] JSME Steam Tables, JSME, Tokyo, 1980.
[19] Silicone Oil Catalog P6-3D, Shin-etsu Chemical Co., Tokyo, 1981.
[20] N. Kaji Direct-contact heat transfer to drops in an intermittent electric field (in Japanese). D.Eng. thesis, Keio University, Yokohama, Japan 1980.
[21] S. Middleman, in: Modeling Axisymmetric Flows, Dynamics of Films, Jets, and Drops, Academic Press, New York, 1995, pp. 260–264.
[22] A.H. Sharbaugh, J.K. Bragg, R.W. Crowe, Dependence of the electric strengths of liquids on electrode spacing, Journal of Applied Physics 26 (1955) 434–437.